Chinese Chemical Letters 35 (2024) 108746

Contents lists available at ScienceDirect

Chinese Chemical Letters

journal homepage: www.elsevier.com/locate/cclet

Remodeling the tumor microenvironment by vascular normalization and GSH-depletion for augmenting tumor immunotherapy

Jin Wang[a], Qingqing Zhang[a], Yanchen Li[a], Xiaoyan Pan[a], Yuanyuan Shan[b,*], Jie Zhang[a,*]

[a] School of Pharmacy, Health Science Center, Xi'an Jiaotong University, Xi'an 710061, China
[b] Department of Pharmacy, The First Affiliated Hospital of Xi'an Jiaotong University, Xi'an 710061, China

ARTICLE INFO

Article history:
Received 4 May 2023
Revised 23 June 2023
Accepted 27 June 2023
Available online 29 June 2023

Keywords:
Vascular normalization
Tumor microenvironment
GSH depletion
Ferroptosis
Activated immune

ABSTRACT

Remodeling tumor microenvironment (TME) is a very promising and effective strategy to enhance the effects of chemotherapy, photodynamic therapy, and immunotherapy. Normalization of tumor vasculature as well as depletion of glutathione (GSH) can improve the TME. Here, we developed a novel therapeutic nanoparticle functional enzyme ultra QDAU5 nanoparticles (FEUQ Nps) based on a fluorescence-on and releasable strategy by combining a vascular normalization inducer, a GSH depleting agent, and an activated fluorophore. In which the cleavage of disulfide bonds releases active molecules that induce vascular normalization and improve the hypoxic microenvironment. In addition, it may deplete GSH in cancer cells, thus inducing the production of reactive oxygen species (ROS) and lipid peroxide (LPO) and promoting iron toxicity. It may also lead to endoplasmic stress and release of calmodulin, which activates the immune system. Meanwhile, quenched fluorophores are turned on in the presence of galactosidase (GLU) for tumor-specific labeling. In summary, we developed novel therapeutic agent nanoparticles with the function of vascular normalization inducers to achieve specific labeling of hepatocellular carcinoma while exerting efficient antitumor effects *in vivo*.

Tumors are surrounded by complex and dynamic microenvironments, which influence their growth, invasion, and metastasis [1,2]. In addition, tumor microenvironment (TME) also contributes to heterogeneity and poses a huge impact on the outcome of cancer treatment [3,4]. Ample studies have firmly established TME reshaping as a very promising and effective strategy to potentiate chemotherapy, photodynamic therapy as well as immunotherapy [5].

Angiogenesis represents a cornerstone of cancer, allowing tumors to receive oxygen and nutrients [6]. The functions of tumor vessels in most cases are abnormal, which leads to a hypoxic TME and hampers the infiltration of immune cells, thus facilitating tumor development and metastasis [7]. Several antiangiogenic drugs have been approved by Food and Drug Administration (FDA) for cancer treatment [8]. However, antiangiogenic drugs possess some intrinsic limitations [9]. For example, some antiangiogenic drugs were reported to induce the production of pro-angiogenic factors and increase the possibility of tumor metastasis and relapse in some cancers [10]. Alternatively, the tumor blood vessels can be remodeled to restore their structure and functions, which is known as vascular normalization [11–13].

In addition to angiogenesis, elevated glutathione (GSH) levels were widely observed in TME among different tumors, which also supports the growth of cancer cells and attenuates the therapeutic efficacy of chemotherapy by its strong antioxidant effects [14]. Evidence has shown that GSH depletion can enhance the efficacy of chemotherapy. Appealingly, recent studies indicated that GSH depletion could also potentiate ferroptosis and immunotherapy [15]. These results present GSH depletion as a promising strategy to remodel the TME.

In addition, for early diagnosis of cancer can have a positive impact on patients. Fluorescent markers are widely used for disease labeling due to their high sensitivity and spatial and temporal resolution, but simple fluorophores lack targeting [16–18]. Therefore, efficient labeling can be achieved by developing smart fluorescent molecules with specific fluorescence turn-on molecules. β-Glucuronidase (β-GLU) is an important biologically active protease that is mainly involved in the degradation of glycosaminoglycans containing glucuronide and is related to various pathophysiological conditions in living organisms [19–22].

Moreover, GLU is also an important tumor biomarker closely related to tumor cell invasion, apoptosis, metastasis, and prolifera-

* Corresponding authors.
E-mail addresses: yuanssyuan@163.com (Y. Shan), zhj8623@mail.xjtu.edu.cn (J. Zhang).

https://doi.org/10.1016/j.cclet.2023.108746
1001-8417/

tion. The expression and activity of GLU in hepatocytes is significantly higher than that in normal hepatocytes when hepatocellular carcinoma becomes cancer [23–25]. Therefore, a novel fluorophore based on GLU intelligent fluorescence turn-on was developed as a tracer molecule. Herein, the free hydroxyl group in the anthocyanin series fluorophore was utilized as the key group to maintain the fluorescence properties, and β-galactosidase (β-Gal) was introduced on the hydroxyl group to quench fluorescence. Under the action of GLU, it was released to turn on fluorescence for specific and intelligent imaging.

Considering the immunosuppressive roles played by angiogenesis and GSH, we speculate that vascular normalization plus GSH depletion might act synergistically to remodel TME to augment tumor immunotherapy. Our lab has a long-lasting interest in developing small-molecule modulators targeting angiogenesis and has discovered several inhibitors with promising vascular normalization effects both *in vitro* and *in vivo*. To construct a molecule with both vascular normalization and GSH-depletion capacity, we designed a bivalent molecule (Fig. S1 in Supporting information). The red moiety was an inhibitor of QDAU5 reported by our group for vascular normalization. The introduction of a thiol acetal group afforded a new inhibitor EQ retaining similar efficacy (Fig. S1 in Supporting information). The disulfide bond was employed as a triggering group in response to GSH, which activates the release of the vascular normalization molecule EQ, and more importantly, eliminates GSH chemically. Meanwhile, we also installed an anthocyanin fluorescent dye (the blue moiety) with the hydroxyl group masked by a galactose moiety. The reasons underlying the introduction of such a moiety are two-fold: Its fluorescence can be switched on in response to overexpressed β-Gal in tumors, and thus the fluorescence can be leveraged as a noninvasive way for diagnosis; the introduction of the hydrophilic galactose moiety makes the title compound amphiphilic, which is anticipated to self-assemble to form nanoparticle for better tumor targeting due to the enhanced permeability and retention (EPR) effect. Expectedly, such a nanomedicine functional enzyme ultra QDAU5 (FEUQ) successfully remodeled vascular morphology and scavenged GSH, improved the hypoxic microenvironment, enhanced ferroptosis, and promoted dendritic cell (DC) maturation. Most importantly, FEUQ displayed very pronounced tumor suppression effects in Hepa1–6 cell tumor-bearing mice *via* stimulating the immune response.

Based on the potential vascular normalization activity of the quinazolinone alkaloid derivative QDAU5, which was discovered in our laboratory in the early stage [26]. Further structural modification was carried out to make it exert more efficient antitumor efficacy based on the regulation of vascular normalization. The disulfide bonds have a certain depleting effect on GSH in the TME. In addition, it also could release other functional molecules in the presence of GSH, which would have less impact on the structure of QDAU5 and can largely preserve its role in promoting vascular normalization while exerting a more efficient anti-tumor effect. Therefore, QDAU5 was structurally optimized by introducing a sulfhydryl group containing a prototype of disulfide bond release to construct a functional molecule (EQ). In addition, to further verify the effect of the modified EQ, the mode of action of EQ and related potential target proteins were investigated and analyzed by molecular docking and cell proliferation inhibition activity assays, and the results showed that the mode of action and preliminary antitumor activity of EQ and QDAU5 with respect to the targets were basically consistent.

The free hydroxyl group is essential for the fluorescence retention of anthocyanin fluorescent dyes. β-Gal was introduced to block the free hydroxyl group as it can be cleaved to release the hydroxyl group under the action of GLU to turn on the fluorescence. Thus, we chose β-Gal to modify the anthocyanin fluorescent dyes to construct the functional fluorescence group. Then, the vascular normalization inducer EQ and disulfide bonds were incorporated to link the fluorescent dyes to construct FEUQ. The chemical structures of functional enzyme ultra linker (FEUL) and FEUQ were validated by proton magnetic resonance (^{1}H NMR) and carbon-13 nuclear magnetic resonance (^{13}C NMR) spectroscopy (Figs. S12–S15 in Supporting information).

The self-assembled nanoparticle formation procedure was completed within 30 min using tetrahydrofuran (THF) as the solvent without an additional catalyst at 1200 rpm at room temperature [27]. The FEUQ nanoparticles (Nps) were prepared by self-assembly in THF-H_2O, and the particle size was detected by dynamic laser scattering (DLS) to be 45 nm with a narrow distribution. In addition, as shown in Fig. S2 (Supporting information), the FEUQ Nps solutions displayed the classical opalescence of nanoformulations (Fig. S2a). Clear vesicle morphology was observed by transmission electron microscopy (TEM), with round regular structures (Fig. S2b). Moreover, the FEUQ Nps formulations exhibited superior storage stability for at least 50 days at 4 °C, as confirmed by monitoring the DLS particle size (Fig. S2c). The outstanding stability typically indicated that the functional molecules do not degrade spontaneously, which is the main factor maintaining the activity of the functional molecules. Next, we explored the release conditions by HPLC under GSH, which showed that EQ released from FEUQ could reach 80% within 20 h under GSH (10 mmol/L, pH 5.0 acetate buffer solution (ABS)). As a result, the high reducing condition of the TME triggered the disassembly of FEUQ Nps, and EQ was released from FEUQ (Fig. S2e).

Subsequently, the cytotoxicity of the FEUQ and FEUQ Nps was evaluated. Low cytotoxicity was observed in normal cells (HEK293) by MTT assay. The results indicated that cell viability was approximately 70% even at a high concentration (20 μmol/L FEUQ, 20 μg/mL FEUQ Nps), suggesting almost no cytotoxicity of the FEUQ and FEUQ Nps (Fig. S2d). After preliminary characterization of the cytotoxicity of nanoparticles *in vitro*, the optical properties of FEUQ Nps in the absence and presence of β-GLU were evaluated in aqueous solution (phosphate-buffered saline (PBS):dimethyl sulfoxide (DMSO) = 7:3 (v:v), pH 7.4, 37 °C). First, the absorption spectra of the FEUL, FEUQ, and FEUQ Nps were evaluated, and the absorption peak appeared at approximately 465 nm (Fig. S2f). Next, in the absence of β-GLU the FEUQ Nps were fluorescent with a weak peak at 545 nm (λ_{em} = 465 nm) (Fig. S2g). In contrast, in the presence of β-GLU, the FEUQ Nps immediately caused a strong fluorescence signal to appear at 545 nm, while the fluorescence intensity increased with increasing enzyme concentration (Fig. S2h, λ_{em} = 465 nm), indicating the ability of the FEUQ Nps to serve as a sensor for β-GLU. Moreover, the FEUQ and FEUQ Nps have consistent fluorescent lighting properties, which indicated that the self-assembly process does not affect the fluorescence turn-on (Fig. S2i).

We investigated the potency of FEUQ Nps on imaging and inhibition of new blood vessel formation. The results indicated that FEUQ Nps could inhibit the formation of new blood vessels and realize imaging of vascular tissue *in vitro*. The formation of new blood vessels was significantly inhibited, and efficient fluorescent labeling could be achieved (Fig. 1a). To explore the effect of different administration treatment junctures, we selected one administration starting point and compared the tumor vasculature alternation on different days. Mice were treated every other day continuously with FEUQ Nps (4 mg/kg) when tumor volumes reached approximately 100–150 mm^3. Herein, the improvement of vascular permeability is an indicator of vascular normalization. Evans blue staining was used to evaluate vascular permeability. The results showed a decrease in Evans blue exudation and an improvement in vascular permeability during the 4th and 6th days of treatment (Fig. 1b). At the same time, immunohistochemistry (IHC) was utilized to evaluate the relevant indicators of tumor vascular nor-

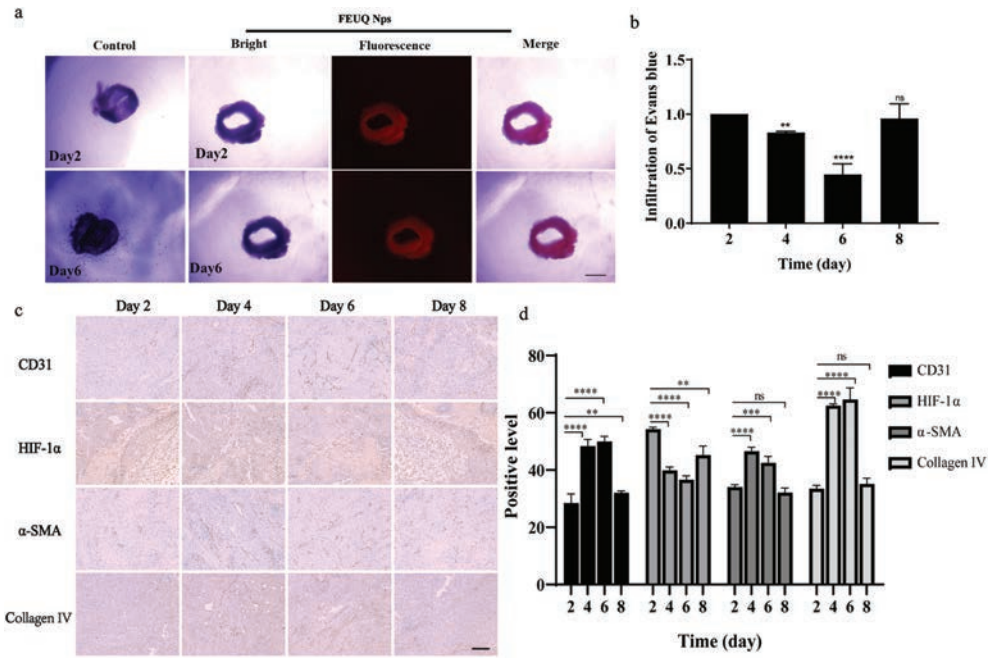

Fig. 1. (a) The effect of the mouse vascular ring after treatment with FEUQ Nps. Scale bar: 20 μm. (b) Vascular permeability assay by Evans blue staining. (c) Immunohistochemical staining of the expression of CD31, α-SMA, collagen IV and HIF-1α in different groups of xenografted tumor tissues after administration of FEUQ Nps at different times. Scale bar: 20 μm. (d) The expression level of HIF-1α, α-SMA, and collagen type IV (collagen IV) was detected by immunohistochemical staining (mean ± standard deviation (SD), *t*-test; $^{**}P < 0.01$, $^{***}P < 0.001$, $^{****}P < 0.0001$ compared to day 2 group, $n = 3$. no significance (ns)).

malization to verify the achievability of FEUQ Nps. Pericytes are the main parietal cells related to vascular endothelial cells (VECs). Neovascularization recruited pericytes to prevent excessive sprouting, stabilize new vasculature, prevent blood vessel leakage, and reshape vasculature into mature vessels. Pericytes (PerC) is considered a reliable indicator for vasculature maturity. Thus, platelet endothelial cell adhesion molecule-31 (CD31), alpha-smooth muscle actin (α-SMA) and collagen type IV (collagen IV) indicated the condition of pericytes and vascular basement membranes. Expression levels reflect the maturity of the vasculature. The higher the expression level, the more mature the blood, and the more complete the vessel and structure. The results showed that after treatment with FEUQ Nps, hypoxiainduciblefactor-1 (HIF-1α) was significantly decreased on the 4th and 6th days of treatment (Figs. 1c and d), whereas the CD31, α-SMA and collagen type IV levels were significantly increased compared with those at other times. Overall, the FEUQ Nps induced abnormal tumor vascularization normalization within 4–6 days. It can be used to define and regulate the vascular normalization time window through the improvement of tumor hypoxic microenvironment indicators by changes in fluorescence signals. It provides a new and convenient method for monitoring the time window of vascular normalization.

The cleavage of disulfide bonds could deplete GSH in the TME, while vascular normalization could improve the hypoxic microenvironment and further reduce the concentration of GSH. The decrease in GSH concentration could induce the production of reactive oxygen species (ROS), resulting in ferroptosis. Meanwhile, it further promoted the production of peroxides, thereby inducing endoplasmic reticulum (ER) stress, secreting calreticulin, promoting antigen presentation, activating the immune system, and exerting an outstanding antitumor effect (Fig. 2a). Therefore, we detected the content of intracellular GSH using a reduced GSH content detection kit. As shown in Fig. 2b, the FEUQ Nps exhibited more significant depletion of GSH than the ferroptosis inducer sorafenib. Otherwise, the disulfide bond is necessary for the depletion of GSH compared with EQ alone and sorafenib. The intracellular GSH level was decreased to 30.78% compared with that of the control group after FEUQ Nps treatment, whereas it only decreased to 46.24% after FEUQ treatment. Sorafenib also exhibited weak GSH depletion ability, further indicating the necessity of the azobenzene group. Accordingly, the complete GSH depletion by FEUQ Nps induced more ROS generation in HepG2 cells, as shown in fluorescence images after staining the intracellular ROS with dichlorodihydro fluorescein diacetate (DCFH-DA, Figs. 2d and e). Furthermore, the azo compounds alone, FEUL, and combinations of these molecules showed only weak effects on the decrease of GSH and increase of LPO (Fig. 2c) and ROS, which further demonstrates the necessity of constructing bifunctional molecules for effective induction of ferroptosis. In addition, FEUQ Nps resulted in significant downregulation of glutathione peroxidase 4 (GPX4, Figs. 2f and g) and upregulation of acyl-CoA synthetase long-chain family member 4 (ACSL4), indicating the effective induction of ferroptosis in tumor cells.

Ferroptosis was also confirmed by the upregulated LPO level in HepG2 cells (Fig. 2b). Next, we also assessed the content of LPO. The results indicated that the content of LPO was significantly increased after treatment with FEUQ Nps. Meanwhile, the increase in LPO and ROS content will cause endoplasmic reticulum stress and secrete calreticulin to activate the immune system. In addition, the improvement of the hypoxic microenvironment contributed to immune activation. Therefore, we investigated and verified the relevant indicators of immune activation. The FEUQ Nps upregulated immunoglobulin heavy chain binding protein (Bip) and C/EBP-homologous protein (CHOP), which indicated the presence of ER stress in tumor cells. ER stress promotes calreticulin production to mediate antigen phagocytosis by tumor immune cells. Therefore, the level of calreticulin in HepG2 cells was explored. As shown in Figs. 2f and g, the production of calreticulin was significantly increased compared with that of sorafenib. Strong induction of immunogenic cell death (ICD) by FEUQ Nps further promoted DC maturation after incubation with HepG2 cell supernatant (Figs. 2h and i). As one of the most important antigen-presenting cell (APC) types, DCs play a crucial role in cancer immunotherapy [28]. The

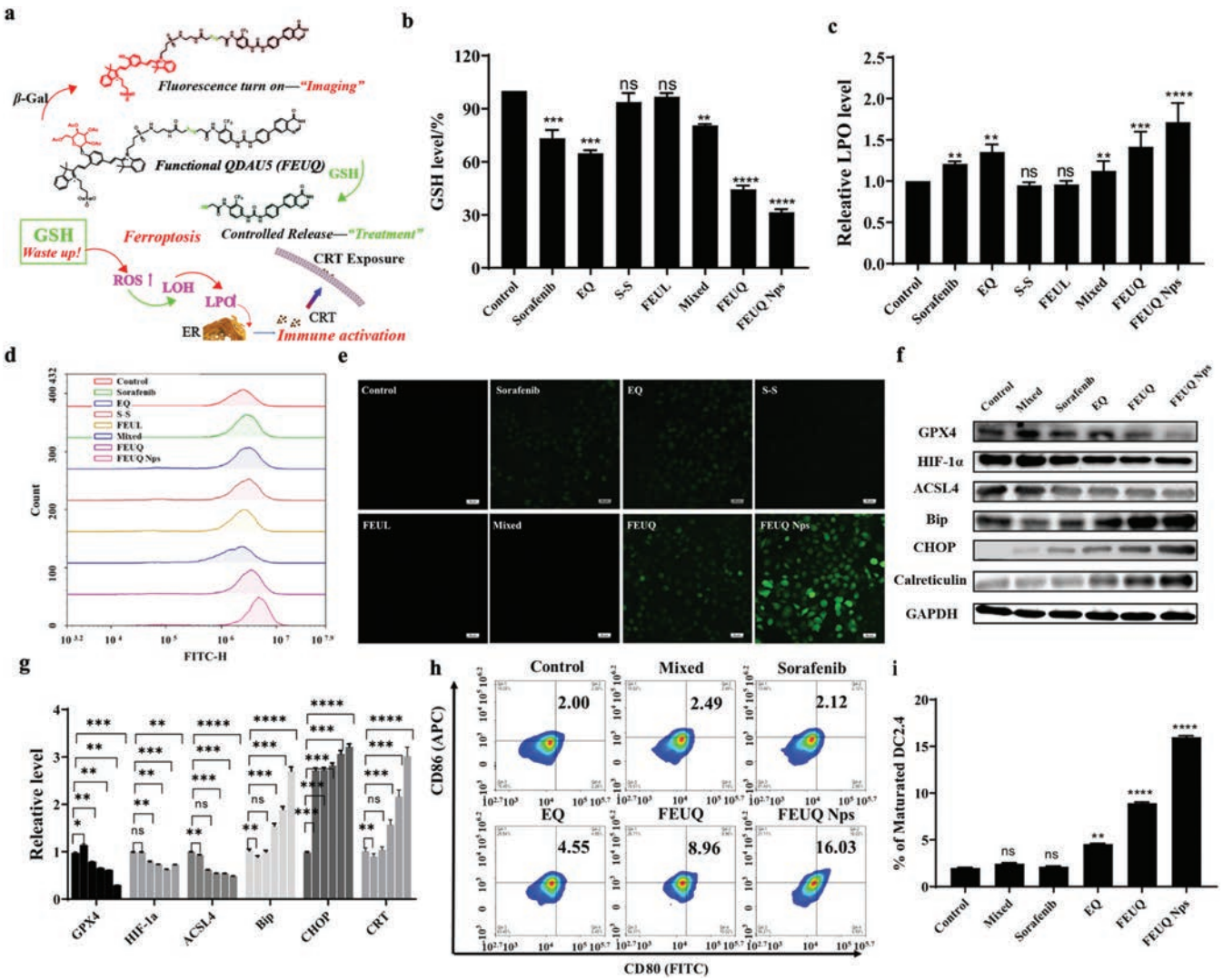

Fig. 2. (a) Mechanism of action of FEUQ. (b) Intracellular GSH levels after different treatments ($n = 3$). (c) Intracellular LPO level detection ($n = 3$). (d) Cell uptake of fluorescence ROS after incubation with dithiodiglycolic acid, FEUL, mixed (azobenzene+ FEUL+ EQ), sorafenib, EQ, FEUQ and FEUQ Nps in HepG2 cells. (e) Fluorescence ROS images of HepG2 cells after incubation with dithiodiglycolic acid, FEUL, mixed (azobenzene+ FEUL+ EQ), sorafenib, EQ, FEUQ and FEUQ Nps. Scale bar: 50 μm. (f, g) Western blot analysis of GPX4, HIF-1α, ACSL4, Bip, and CHOP expression. (h, i) CRT exposure of HepG2 cells after treatment with Mixed (Azobenzene+ FEUL+ EQ), sorafenib, EQ, FEUQ and FEUQ Nps (mean ± SD, *t*-test; $^{**}P < 0.01$, $^{***}P < 0.001$, $^{****}P < 0.0001$ compared to control group, $n = 3$). GAPDH, glyceraldehyde-3-phosphate dehydrogenase.

DC maturation rate of the FEUQ Nps group was as high as 16.03%, which was much higher than that of the control (2.00%). Moreover, the benefit of combination therapy in enhancing immune activation was confirmed to be weaker in the combination therapy group (2.49%) than in the FEUQ group (8.96%), reinforcing the benefit of disulfide bond modification of EQ to build FEUQ functional molecules that exert stronger immune activation potency.

Subsequently, we evaluated the *in vivo* therapeutic efficacy of FEUQ Nps in Hepa1–6 cell tumor-bearing mice. Animal welfare and experimental procedures have been reviewed and approved by the Animal Ethics Committee of Xi'an Jiaotong University. The treatment schedule is shown in Fig. 3a, where the FEUQ Nps were administered in doses of 4 mg/kg on Days 0, 2, 4, 6, 8, 10 and 12 by intravenous (i.v.) injection. As shown in Fig. 3g, no evident weight loss, histopathological damage or death was observed among the various treatment groups, suggesting negligible cytotoxicity of the FEUQ Nps (Fig. S11 in Supporting information). Moreover, vigorous tumor growth inhibition was observed in the mice treated with nanoparticles (average tumor volume ≈ 150 mm^3) after 12 days, whereas the average tumor volume in the mice treated with PBS reached 150 mm^3 and was 8-fold larger than that on the first day (1200 mm^3). The tumor weight and tumor image on the 12th day further revealed the extraordinary antitumor efficacy of FEUQ Nps (Figs. 3e and f). We also evaluated the effect of ferroptosis in tumors. GPX4 downregulation (Fig. 3b), GSH depletion (Fig. 3c), and LPO upregulation (Fig. 3d) were validated in tumor tissue, confirming *in vivo* ferroptosis induction by FEUQ Nps. Moreover, we investigated and verified the relevant indicators of immune activation. The FEUQ Nps upregulated Bip and CHOP, which indicated the presence of ER stress *in vivo* (Fig. S13 in Supporting information). In addition, we analyzed the immune activation in tumors on Day 10 after the first injection, $CD8^+$ T cells, as the central effector T cells, were analyzed by flow cytometry. As shown in Figs. 3h and i, the tumor infiltration of $CD8^+$ T cells was limited to 4.22% in the control group, and the sorafenib treatments only generated weak immune responses, where the $CD8^+$ T-cell ratios were limited to 8.20%. To our surprise, the FEUQ Nps significantly improved immune activation and promoted the infiltration of $CD8^+$ T cells to 66.46% in tumor tissue. These results validated that the FEUQ Nps could effectively boost immune activation in tumors. In ad-

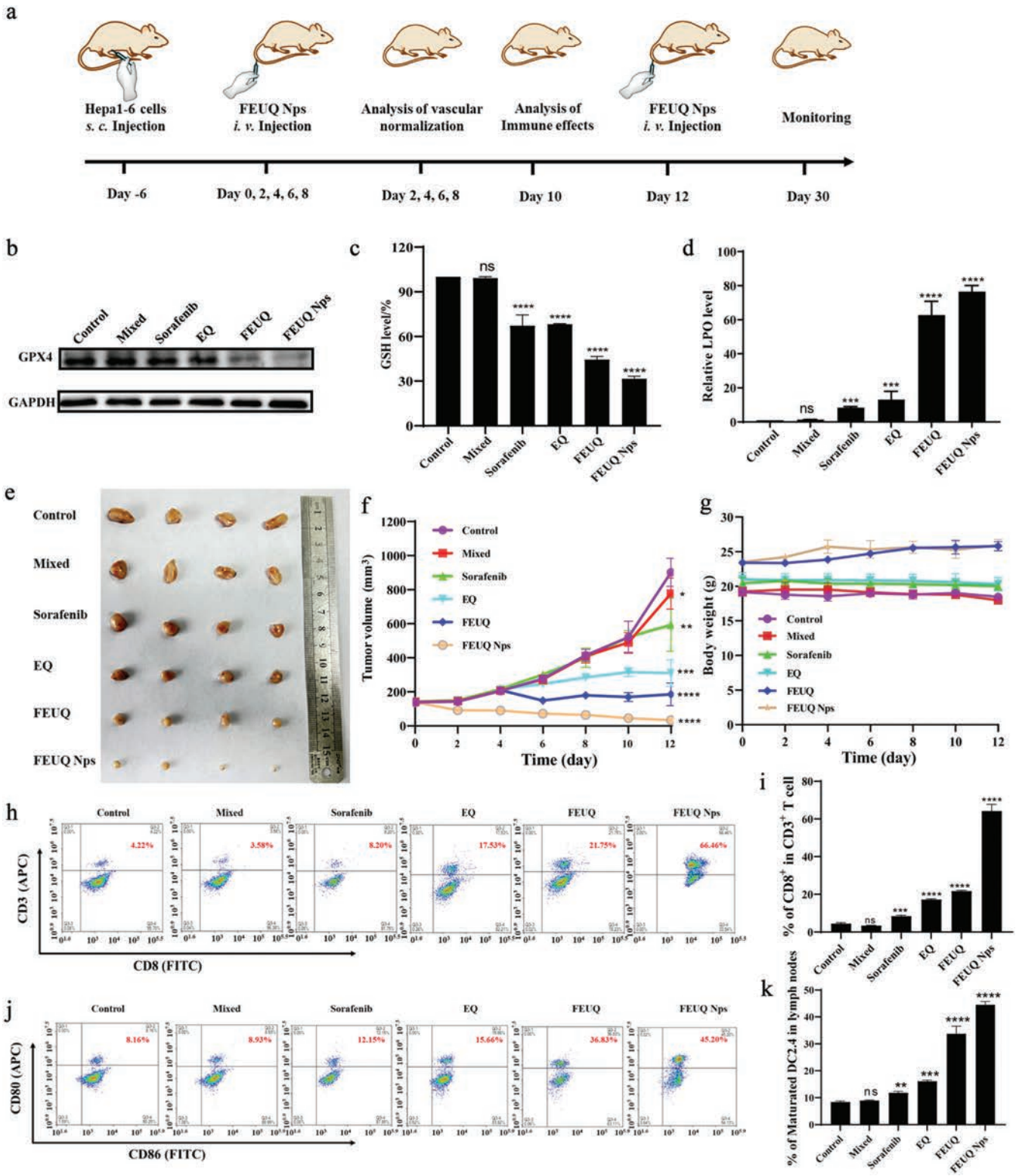

Fig. 3. (a) Treatment schedule of FEUQ Nps. (b) Western blot analysis of GPX4 expression *in vivo*. (c) GSH level after different treatments *in vivo*. (d) LPO level after different treatments *in vivo*. (e) Representative images of *ex vivo* tumors on Day 12. (f) Tumor growth curve of the Hepa1-6 model after treatment with mixed, sorafenib, EQ, FEUQ and FEUQ Nps. (g) The body weight curve of the Hepa1-6 model after treatment with sorafenib, EQ, FEUQ and FEUQ Nps. (h, i) Infiltration of $CD8^+$ T cells in tumors, as analyzed by flow cytometry. (j, k) DC maturation in lymph nodes on Day 10 (*t*-test, compared to control group, $^{**}P < 0.01$, $^{***}P < 0.001$, $^{****}P < 0.0001$). Data are represented as mean ± SD ($n = 3$).

dition, DC maturation in lymph nodes (LNs) was also evaluated by flow cytometry by analyzing the ratio of $CD80^+$ $CD86^+$ cells. Expectantly, FEUQ Nps also induced the highest percentage of DC maturation (45.20%) compared with the control group (8.16%) (Figs. 3j and k). It should be noted that the strong ferroptosis induction and immune activation by FEUQ Nps completely prevented liver carcinoma cells.

In conclusion, a novel theranostic nanoparticle functionalized with a vascular normalization inducer has been developed. This novel theranostic nanoplatform could be utilized for the early diagnosis and therapy of liver cancer *in vivo*. The bifunctional nanoparticles exhibited a great optical response to β-Gal with high sensitivity and selectivity. Otherwise, combined with a releasable strategy, active molecules (EQ) could be released to induce vascular normalization and improve the hypoxic TME while depleting GSH, inducing ferroptosis, and activating the immune system. As expected, the FEUQ Nps could induce abnormal tumor vascularization to normalize within 4–6 days and improve the hypoxic TME. Meanwhile, cleavage of disulfide bonds led to the massive depletion of GSH in cellular tissues, resulting in overproduction of ROS and LPO, inducing ferroptosis. At the same time, the increasement of ROS and LPO will induce ER stress to release calreticulin, which promotes the maturation of DC cells and $CD8^+$ T cells. More importantly, these bifunctional theranostic nanoparticles could be used for dynamic monitoring and imaging of liver cancer. Overall, our findings proposed a promising strategy for imaging and treating liver cancer by responding to β-Gal, inducing vascular normalization, converting the hypoxic microenvironment, enhancing ferroptosis and activating immunity *in vivo*. In the future, it has the potential to be used as a solution for the early diagnosis and therapy of liver cancer.

Declaration of competing interest

The authors declare that they have no known competing financial interests or personal relationships that could have appeared to influence the work reported in this paper.

Acknowledgments

This work was supported by the National Natural Science Foundation of China (NSFC, No. 82173742), the Science Fund for Distinguished Young Scholars of Shaanxi Province (No. 2022JC-54), and the Key Research and Development Program of Shaanxi Province (No. 2023-YBSF-131).

Supplementary materials

Supplementary material associated with this article can be found, in the online version, at doi:10.1016/j.cclet.2023.108746.

References

[1] J. Hu, X. Yuan, F. Wang, et al., Chin. Chem. Lett. 32 (2021) 1341–1347.
[2] Y. Chu, T. Sun, C. Jiang, Chin. Chem. Lett. 33 (2022) 4157–4168.
[3] S. Chen, X. Zhang, Y. Yu, J. Wang, Chin. Chem. Lett. 32 (2021) 3043–3047.
[4] D. He, M. Yan, P. Sun, et al., Chin. Chem. Lett. 32 (2021) 2994–3006.
[5] M. Li, X. Wang, Y. Wang, et al., Front. Pharmacol. 12 (2021) 797634.
[6] S. Wen, K. Zhang, Y. Li, et al., Chin. Chem. Lett. 31 (2020) 3153–3157.
[7] M. Valdivielso-Ramos, A. Martin-Santiago, J.M. Azaña, et al., Clin. Exp. Dermatol. 46 (2021) 300–305.
[8] M.E. Cabanillas, M. Ryder, C. Jimenez, Endocr. Rev. 40 (2019) 1573–1604.
[9] M. Visagie, A. Theron, T. Mqoco, et al., PLoS One 8 (2013) e71935.
[10] I. Larionova, E. Kazakova, T. Gerashchenko, et al., Cancers 13 (2013) 3253.
[11] W.J. Paulus, C. Tschöpe, J. Am. Coll. Cardiol. 62 (2013) 263–271.
[12] C. Viallard, B. Larrivée, Angiogenesis 20 (2017) 409–426.
[13] L. Marzi, A. Mega, S. Gitto, et al., Cancers 14 (2022) 3332.
[14] S. Wang, H. Liao, F. Li, D. Ling, Chin. Chem. Lett. 30 (2019) 847–852.
[15] Z. Zhou, H. Liang, R. Yang, et al., Angew. Chem. Int. Ed. 61 (2022) e202202843.
[16] A. Batista, H.G. Breunig, A. König, et al., J. Biomed. Opt. 23 (2018) 1–8.
[17] K. Konig, I. Riemann, J. Biomed. Opt. 8 (2003) 432–439.
[18] V. Ulrich, P. Fischer, I. Riemann, et al., Scanning 26 (2004) 217–225.
[19] R.A. Jefferson, T.A. Kavanagh, M.W. Bevan, EMBO J. 6 (1987) 3901–3907.
[20] M. de Graaf, E. Boven, H.W. Scheeren, et al., Curr. Pharm. Des. 8 (2002) 1391–1403.
[21] Y. Xianyu, S. Su, J. Hu, et al., Biosens. Bioelectron. 190 (2021) 113430.
[22] H.S. Lazarus, W.S. Sly, J.W. Kyle, et al., Exp. Eye Res. 56 (1993) 531–541.
[23] Y. Liu, M. Pan, W. Wang, et al., Anal. Chem. 91 (2019) 2086–2092.
[24] Q. Shi, G.R. Haenen, L. Maas, et al., Arch. Toxicol. 90 (2016) 2261–2273.
[25] L.L. Fan, Y.W. Feng, J. Bian, et al., Chin. Chem. Lett. (2023), doi:10.1016/j.cclet.2023.108443.
[26] B. Dai, X. Shi, N. Ma, et al., J. Cell. Mol. Med. 22 (2018) 5231–5243.
[27] P. Liang, X. Huang, Y. Wang, et al., ACS Nano 12 (2018) 1446–11457.
[28] X. Heng, R. Feng, L. Zhu, et al., Chin. Chem. Lett. 33 (2022) 4331–4334.